Bioresource Technology 178 (2015) 53–64

Contents lists available at ScienceDirect

Bioresource Technology

journal homepage: www.elsevier.com/locate/biortech

Metal catalysts for steam reforming of tar derived from the gasification of lignocellulosic biomass

Dalin Li [a,*], Masazumi Tamura [b], Yoshinao Nakagawa [b], Keiichi Tomishige [b]

[a] National Engineering Research Center of Chemical Fertilizer Catalyst (NERC-CFC), School of Chemical Engineering, Fuzhou University, Gongye Road 523, Fuzhou 350002, Fujian, PR China

[b] Department of Applied Chemistry, School of Engineering, Tohoku University, 6-6-07, Aoba, Aramaki, Aoba-ku, Sendai 980-8579, Japan

HIGHLIGHTS

- Metal catalysts including Rh, Ni, and Co are efficient for steam reforming of tar.
- Presence of reducible oxides and second metals is effective to improve performance.
- Synergy effects on metal-oxide and metal–metal interface can play an important role.
- Hydrotalcite precursors are promising to prepare high-performance metal catalyst.

GRAPHICAL ABSTRACT

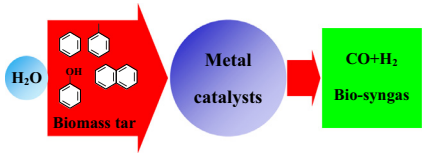

ARTICLE INFO

Article history:
Received 8 August 2014
Received in revised form 30 September 2014
Accepted 2 October 2014
Available online 13 October 2014

Keywords:
Biomass gasification
Tar
Steam reforming
Metal catalysts
Synthesis gas

ABSTRACT

Biomass gasification is one of the most important technologies for the conversion of biomass to electricity, fuels, and chemicals. The main obstacle preventing the commercial application of this technology is the presence of tar in the product gas. Catalytic reforming of tar appears a promising approach to remove tar and supported metal catalysts are among the most effective catalysts. Nevertheless, improvement of catalytic performances including activity, stability, resistance to coke deposition and aggregation of metal particles, as well as catalyst regenerability is greatly needed. This review focuses on the design and catalysis of supported metal catalysts for the removal of tar in the gasification of biomass. The recent development of metal catalysts including Rh, Ni, Co, and their alloys for steam reforming of biomass tar and tar model compounds is introduced. The role of metal species, support materials, promoters, and their interfaces is described.

1. Introduction: gasification of lignocellulosic biomass

In recent decades, biomass has received worldwide interest due to its great potential to substitute fossil fuels for the production of electricity, fuels, and chemicals (Huber et al., 2006). Compared to fossil fuels, biomass has several significant advantages including its abundance, renewability, and carbon-neutrality as well as low sulfur content. A number of technologies including biochemical and thermochemical processes are currently under development for the conversion of biomass to energy. Among them, gasification of biomass is one of the most economical and efficient technologies for the conversion of lignocellulosic biomass (Lasa et al., 2011; Peter, 2002). The product gas or synthesis gas ($CO + H_2$) produced from gasification of biomass has a wide applications. It can not only be used for the generation of electricity and heat by direct combustion in internal combustion engines, but also an important feedstock in C1 chemistry for the production of hydrogen, liquid hydrocarbon fuels, and methanol.

* Corresponding author. Tel.: +86 595 83731234.
E-mail address: dalinli@fzu.edu.cn (D. Li).

http://dx.doi.org/10.1016/j.biortech.2014.10.010
0960-8524/

However, the raw product gas from the biomass gasifier contains many contaminants such as particulates, alkali compounds, tars, nitrogen-containing compounds and sulfur. Particularly, the presence of tar in the product gas is highly undesirable. Tar is a complex mixture of condensable hydrocarbons, including single-ring to five-ring aromatic compounds along with other oxygen-containing hydrocarbons and polycyclic aromatic hydrocarbon (PAH). Tar formation represents a decrease in the gasification efficiency since less of the biomass is converted to a fuel or synthesis gas. More importantly, tar can condense in the gasifier pipe outlets and in particulate filters, which leads to blockages and filter clogging. Tar causes further downstream problems and clogs fuel lines and injectors in internal combustion engines. Meanwhile, tar can cause serious coke deposition on the downstream catalysts leading to rapid deactivation if the synthesis gas is utilized for the production of methanol and Fischer–Tropsch liquids.

Several strategies including physical separation (such as filtration and aqueous or liquid scrubbing), thermal cracking, and catalytic tar conversion, have been investigated to remove tar from the product gas. Compared to physical separation and thermal cracking, catalytic tar conversion appears more promising, because it can convert tar into synthesis gas at the same or even lower temperature than the gasification and without the production of wastewater, which will improves the carbon efficiency and entire process efficiency. Catalytic tar conversion can proceed in two ways: one approach is incorporating or mixing catalyst with the biomass to achieve so-called catalytic gasification or pyrolysis (primary methods), where tar is removed in the gasifier; in the other approach, the gasifier producer gas is treated downstream of the gasifier in a secondary reactor (secondary methods), where the tar is removed outside the gasifier.

So far many types of catalysts have been tested for tar conversion, such as calcined rocks, olivine, clay minerals, ferrous metal oxides, char, FCC (Fluid Catalytic Cracking) catalysts, alkali metal carbonates, activated alumina, supported-metal catalysts (Abu El-Rub et al., 2004; Xu et al., 2010; Yung et al., 2009). Despite the higher price, supported-metal catalysts such as Rh, Ni, and Co have attracted much attention because of their high activity for catalytic tar reforming at low temperatures. Moreover, these metal catalysts are active for catalytic reforming of methane and other light hydrocarbons, which is beneficial to produce more syngas and adjust the syngas composition. It has also been reported that metal catalysts like Ni can catalyze the decomposition of NH_3 contaminant, reducing the amount of NH_3 in product gas (Xu et al., 2010). However, the metal catalysts may suffer from deactivation due to sintering, coke deposition, and poisoning with sulfur, chlorine, and alkali metals. Coke deposition is one of the most serious issues in catalytic reforming of hydrocarbons, especially for aromatic hydrocarbons. Catalyst regeneration by coke removal, such as through combustion, would be necessary. However, it often causes aggregation and structural changes in the metal particles during oxidation and/or subsequent reduction treatments, leading to poor activity and a short catalyst life (Li et al., 2013; Nakamura et al., 2009). Therefore, considerable efforts have been devoted to the development of efficient metal catalyst with high activity and stability for the tar reforming.

In recent years, a number of supported metal catalysts have been developed and some of them have been applied to the tar removal on pilot-scale biomass gasification facilities (Basile et al., 2011; Hofbauer et al., 2002; Pfeifer et al., 2004). In this review, we focus on the design and catalysis of supported metal catalysts for steam reforming (SR) of tar and its model compounds, with an aim to understand the fundamental relation between the structure and catalytic performance. The role of metal species, support materials, promoters, and their interfaces etc. is described, and we hope this review article will contribute to the future catalyst development. The scaling-up applications of metal catalysts in the biomass gasification are not mentioned in detail in this review.

2. Tar model compounds for catalyst development

To make a careful investigation on the catalyst performance and gain insight to the metal catalysis, tar model compounds are usually chosen. The most widely investigated tar model compounds include benzene, toluene, naphthalene, and phenol, which are typical one- and two-ring aromatic hydrocarbons and oxygen-containing aromatic hydrocarbons. Tables 1–3 list some representative catalyst systems for SR of benzene, toluene, naphthalene, and phenol, respectively.

2.1. Steam reforming of benzene and toluene over metal catalysts

Colby et al. studied the activity of Rh and Rh–Ce catalysts supported on α-Al_2O_3 foam monoliths for the SR of benzene (Colby et al., 2009). Benzene conversion exhibited a strong dependence on temperature and H_2O concentration in the feed. Promotion of Rh-based catalysts with Ce leads to an increase of the Rh dispersion and better stability for benzene SR. The Rh–Ce catalyst showed almost complete C_6H_6 conversion for a biomass-derived syngas mixture of N_2, H_2, CO, CO_2, H_2O, and C_6H_6 at 1123 K. A reaction scheme of benzene SR was proposed. C_6H_6 adsorbed onto Rh metal undergoing C–H or C–C bond cleavage to form surface carbon (C^*) and H_2. Reaction of C^* took place with hydroxyl groups derived from the dissociation of H_2O on the support to form OH^* and H^*. H_2O might also react with ceria in its reduced state, donating oxygen to the ceria lattice to form H_2. The OH^* groups transferred to the Rh metal to react with C^* to form CO. The addition of ceria could increase the rate of hydroxyl transfer between the oxide support and metal. The C^* on the metal surface could be oxidized through a redox cycle in which ceria was oxidized by an oxygen containing species on the surface and then transferred oxygen to the metal catalyst. This might contribute to the large improvement in catalyst performance by adding Ce to the Rh catalyst. Similar role of Ce on the supply of oxygen has been reported for $Rh/CeO_2/SiO_2$, which was very effective to the gasification of wood biomass with air in the fluidized bed reactor, where CeO_2 played an important role in the supply of oxygen species to Rh metal surface (Asadullah et al., 2002).

Mei et al. conducted a comparative investigation on the activity of $MgAl_2O_4$-supported Rh and Ir catalysts for benzene SR (Mei et al., 2013). It was reported that both 5% $Rh/MgAl_2O_4$ and 5% $Ir/MgAl_2O_4$ catalysts were highly active for benzene SR in the temperature range of 973–1123 K. Higher benzene turnover frequency and conversion were observed for the $Rh/MgAl_2O_4$ catalyst. It was found that at steam/carbon >12, the benzene conversion was only a weak function of the H_2O concentration in the feed, suggesting that the initial benzene decomposition step, rather than the benzene adsorption, was most likely the rate-determining step over supported Rh and Ir catalysts. The DFT study of initial benzene decomposition over two supported model catalysts suggested that benzene decomposition was more facile on Rh catalysts. The C–C and the C–H bond scissions of benzene on the Rh(1 1 1) and the Rh_{50} cluster were competitive, while the C–C bond scission was slightly more favorable on the Ir(1 1 1) surface and the Ir_{50} cluster. It was also shown that benzene decomposition was kinetically favorable on the small clusters rather than on the larger particles.

Park et al. investigated the effects of support, Ni-precursor, and Ni loading on the catalytic performance in SR of benzene (Park et al., 2010). The activity order in terms of benzene conversion was $Ni/CeO_2–ZrO_2 > Ni/\gamma\text{-}Al_2O_3 > Ni/CeO_2 > Ni/ZrO_2$. The high performance of $Ni/CeO_2–ZrO_2$ was attributed to its greater redox

Table 1
Steam reforming of benzene and toluene over supported-metal catalysts.

Catalyst	Metal loading (wt%)	Preparation method[a]	Model compound	Reaction conditions	Conversion (%)	Refs.
$Rh/\alpha\text{-}Al_2O_3$	0.5	iw	Benzene	S/C = 1.67, GHSV = 52,900 h^{-1}, T = 1123 K	49.8	Colby et al. (2009)
$Rh–CeO_2/\alpha\text{-}Al_2O_3$	0.5	iw	Benzene	S/C = 1.67, GHSV = 52,900 h^{-1}, T = 1123 K	99.8	Colby et al. (2009)
$Rh/MgAl_2O_4$	5	iw	Benzene	S/C = 12, GHSV = 220,000 h^{-1}, T = 973 K	~65	Mei et al. (2013)
$Ir/MgAl_2O_4$	5	iw	Benzene	S/C = 12, GHSV = 220,000 h^{-1}, T = 973 K	~56	Mei et al. (2013)
$Ni/\gamma\text{-}Al_2O_3$	15	imp	Benzene	S/C = 2.4, W/F = 19.6 g h mol^{-1}, T = 973 K	82.5	Park et al. (2010)
Ni/ZrO_2	15	imp	Benzene	S/C = 2.4, W/F = 19.6 g h mol^{-1}, T = 973 K	38.8	Park et al. (2010)
Ni/CeO_2	15	imp	Benzene	S/C = 2.4, W/F = 19.6 g h mol^{-1}, T = 973 K	57.7	Park et al. (2010)
$Ni/CeO_2–ZrO_2$	15	imp	Benzene	S/C = 2.4, W/F = 19.6 g h mol^{-1}, T = 973 K	87.2	Park et al. (2010)
Ni/olivine	3.9	imp	toluene	S/C = 2.3, $W/F_{toluene}$ = 9 kg h m^{-3}, T = 923 K	100	Swierczynski et al. (2007)
$Ni/LaAlO_3$	10	imp	toluene	S/C = 3, W/F = 13.5 g h mol^{-1}, T = 873 K	81	Sekine et al. (2013)
$Ni/LaFeO_3$	10	imp	Toluene	S/C = 3, W/F = 13.5 g h mol^{-1}, T = 873 K	55	Sekine et al. (2013)
$Ni/BaTiO_3$	10	imp	Toluene	S/C = 3, W/F = 13.5 g h mol^{-1}, T = 873 K	41	Sekine et al. (2013)
$Ni/SrTiO_3$	10	imp	Toluene	S/C = 3, W/F = 13.5 g h mol^{-1}, T = 873 K	65	Sekine et al. (2013)
$Ni/LaCeO_3$	10	imp	Toluene	S/C = 3, W/F = 13.5 g h mol^{-1}, T = 873 K	66	Sekine et al. (2013)
$Ni/LaAlO_3$	5	imp	Toluene	S/C = 2, W/F = 3.4 g h mol^{-1}, T = 873 K	25.8	Sekine et al. (2013)
Ni/La_2O_3	5	imp	Toluene	S/C = 2, W/F = 3.4 g h mol^{-1}, T = 873 K	14.0	Sekine et al. (2013)
$Ni/\alpha\text{-}Al_2O_3$	5	imp	Toluene	S/C = 2, W/F = 3.4 g h mol^{-1}, T = 873 K	6.3	Sekine et al. (2013)
$Ni/\gamma\text{-}Al_2O_3$	5	imp	Toluene	S/C = 2, W/F = 3.4 g h mol^{-1}, T = 873 K	29.7	Sekine et al. (2013)
$Ni/La_{0.7}Sr_{0.3}AlO_{3-\delta}$	5	imp	Toluene	S/C = 2, W/F = 3.4 g h mol^{-1}, T = 873 K	58.2	Sekine et al. (2013)
$Ni/La_{0.7}Sr_{0.3}AlO_{3-\delta}$	10	imp	Toluene	S/C = 2, W/F = 3.4 g h mol^{-1}, T = 873 K	57.2	Sekine et al. (2013)
$Ni/La_{0.9}Ba_{0.1}AlO_{3-\delta}$	10	imp	Toluene	S/C = 2, W/F = 3.4 g h mol^{-1}, T = 873 K	56.4	Sekine et al. (2013)
$Ni/La_{0.9}Ca_{0.1}AlO_{3-\delta}$	10	imp	Toluene	S/C = 2, W/F = 3.4 g h mol^{-1}, T = 873 K	42.5	Sekine et al. (2013)
$Pt/Ni/La_{0.7}Sr_{0.3}AlO_{3-\delta}$	5	imp	Toluene	S/C = 2, W/F = 3.4 g h mol^{-1}, T = 873 K	–	Mukai et al. (2014)
$LaNi_{0.8}Fe_{0.2}O_3$	20	Citric acid sol–gel	Toluene	S/C = 3.4, W/F = 3 g h mol^{-1}, T = 923 K	53.1	Oemar et al. (2013)
$La_{0.8}Mg_{0.2}Ni_{0.8}Fe_{0.2}O_3$	20	Citric acid sol–gel	Toluene	S/C = 3.4, W/F = 3 g h mol^{-1}, T = 923 K	22.1	Oemar et al. (2014)
$La_{0.8}Ca_{0.2}Ni_{0.8}Fe_{0.2}O_3$	20	Citric acid sol–gel	Toluene	S/C = 3.4, W/F = 3 g h mol^{-1}, T = 923 K	43.7	Oemar et al. (2014)
$La_{0.8}Sr_{0.2}Ni_{0.8}Fe_{0.2}O_3$	20	Citric acid sol–gel	Toluene	S/C = 3.4, W/F = 3 g h mol^{-1}, T = 923 K	48.0	Oemar et al. (2014)
$Ni/Fe_2O_3–Al_2O_3$	10	imp	Toluene	S/C = 3.4, W/F = 3 g h mol^{-1}, T = 923 K	80.9	Ashok and Kawi (2013)
Ni–Fe/Mg/Al	12	cp	Toluene	S/C = 1.7, W/F = 0.05 g h mol^{-1}, T = 873 K	83.2	Koike et al. (2012)
Ni/Mg/Al	12	cp	Toluene	S/C = 1.7, W/F = 0.05 g h mol^{-1}, T = 873 K	53.3	Koike et al. (2012)
$Ni–Fe/\alpha\text{-}Al_2O_3$	12	co-iw	Toluene	S/C = 1.7, W/F = 0.05 g h mol^{-1}, T = 873 K	26.3	Koike et al. (2012)
$Ni/\alpha\text{-}Al_2O_3$	12	iw	Toluene	S/C = 1.7, W/F = 0.05 g h mol^{-1}, T = 873 K	26.5	Koike et al. (2012)
$Ni–Co/\alpha\text{-}Al_2O_3$	12	co-iw	Toluene	S/C = 3.4, W/F = 0.03 g h mol^{-1}, T = 923 K	59.0	Wang et al. (2013)
$Co–Fe/\alpha\text{-}Al_2O_3$	12	co-iw	Toluene	S/C = 3.4, W/F = 0.05 g h mol^{-1}, T = 873 K	68.2	Koike et al. (2013a)
$Ni/\alpha\text{-}Al_2O_3$	12	iw	Toluene	S/C = 3.4, W/F = 0.03 g h mol^{-1}, T = 923 K	54.2	Wang et al. (2013)
$Co/\alpha\text{-}Al_2O_3$	12	iw	Toluene	S/C = 3.4, W/F = 0.03 g h mol^{-1}, T = 923 K	81.4	Wang et al. (2013)
$Ni/Ca_{12}Al_{14}O_{33}$	5	Solid mixing	Toluene	S/C = 2.2, GHSV = 6,000 h^{-1}, T = 823 K	77.4	Li et al. (2009)
$Ni/LaAl_{11}O_{18}$	6	imp	Toluene	S/C = 1.9, WHSV = 20,000 mL g^{-1} h^{-1}, T = 923 K	68	Quitete et al. (2014)
$Ni/La_{0.8}Ce_{0.2}Al_{11}O_{19}$	6	imp	Toluene	S/C = 1.9, WHSV = 20,000 mL g^{-1} h^{-1}, T = 923 K	76	Quitete et al. (2014)
$Ni/CaAl_{12}O_{19}$	6	imp	Toluene	S/C = 1.9, WHSV = 20,000 mL g^{-1} h^{-1}, T = 923 K	79	Quitete et al. (2014)
$Ni + MnO_x/Al_2O_3$	12	co-iw	Toluene	S/C = 3.4, W/F = 0.2 g h mol^{-1}, T = 873 K	~100	Koike et al. (2013b)

[a] iw: incipient wetness method, imp: impregnation method, co-iw: co-incipient wetness method, cp: co-precipitation method.

characteristics. With the exception of nickel nitrate, all the Ni-precursors (chloride and sulfate) caused deactivation of the catalyst. Similar effect of the Ni precursors has been observed on the Ni catalysts for methane reforming (Li et al., 2005).

Courson and co-workers have developed a Ni/olivine catalyst for fluidized bed steam gasification of biomass. Study of the effect of the preparation parameters showed that optimized Ni/olivine catalyst was prepared with 3.9 wt% Ni using nickel nitrate as precursor and calcined at 1373 K (Swierczynski et al., 2007). On the optimized catalyst, total toluene conversion was obtained at reaction temperature $T \geqslant 923$ K under S/C = 2.3 and $W/F_{toluene}$ = 9 kg h m^{-3}, and carbon formation was negligible. The catalyst stability resulting from coke resistance was explained by the formation of active Ni–Fe/MgO/olivine system (Swierczynski et al., 2006). The formation of Ni–Fe alloys was confirmed by TEM after the SR of toluene, where Ni–Fe particles with a variable Ni/Fe ratio and mean size of 50–200 nm were observed. It was suggested that MgO enhanced steam adsorption, facilitating the gasification of surface carbon and that Ni–Fe alloys prevented carbon deposition by dilution effect. On the other hand, it is noted that the composition of the Ni–Fe particles varied in a wide range from rich in nickel to rich in iron, and the particle sizes were quite large. A careful control of the particle's composition and size would be desirable to further improve the catalytic performance.

Sekine and co-workers conducted considerable works on the development of Ni/perovskite catalysts. It was reported (Sekine et al., 2013) that the $Ni/LaAlO_3$ catalyst showed higher catalytic activity in SR of toluene than Ni/La_2O_3, $Ni/\alpha\text{-}Al_2O_3$, and other perovskite-supported catalysts like $Ni/LaFeO_3$, $Ni/BaTiO_3$, $Ni/SrTiO_3$, and $Ni/LaCeO_3$. Partial substitution of the La site of $LaAlO_3$ support with other elements (Sr, Ba or Ca) showed that substitution with 30% Sr promoted catalytic activity and selectivity to hydrogen. The Ni loading amount over $Ni/La_{0.7}Sr_{0.3}AlO_{3-\delta}$ catalyst was optimized to be 5 wt%. The catalytic performance of 5 wt% $Ni/La_{0.7}Sr_{0.3}AlO_{3-\delta}$ was even better than Rh-supported catalysts (1 wt% $Rh/\gamma\text{-}Al_2O_3$, $Rh/LaAlO_3$, and $Rh/La_{0.7}Sr_{0.3}O_{3-\delta}$). It was also found that substituting Sr in the $LaAlO_3$ perovskite had a strong promoting effect for the catalytic activity and coke-suppression, while impregnating Sr showed no such promoting effect. Transient response test with $H_2^{18}O$ revealed the formation of ^{18}O-containing products on the $Ni/La_{0.7}Sr_{0.3}AlO_{3-\delta}$ catalyst derived from redox between the lattice oxygen in the perovskite and water (Mukai et al., 2013). The amount of surface oxygen vacancies might be related to the lattice oxygen mobility. Based on results of the dependence of the reaction rate on the partial pressure of H_2O on Ni/perovskite catalyst, the reaction rates were about a first-order relation to the partial pressure of H_2O at low temperature and zero order at high temperature. In contrast, the dependence of toluene was zero at

Table 2
Steam reforming of naphthalene over supported-metal catalysts.

Catalyst	Metal loading (wt%)	Preparation method[a]	Model compound	Reaction conditions	Conversion (%)	Refs.
Pt/CeO_2	1	imp	Naphthalene/benzene	S/C = 1, GHSV = 19,200 h^{-1}, T = 1073 K	20	Furusawa et al. (2013)
Pt/ZrO_2	1	imp	Naphthalene/benzene	S/C = 1, GHSV = 19,200 h^{-1}, T = 1073 K	0	Furusawa et al. (2013)
Pt/MgO	1	imp	Naphthalene/benzene	S/C = 1, GHSV = 19,200 h^{-1}, T = 1073 K	51.3	Furusawa et al. (2013)
Pt/Al_2O_3	1	imp	Naphthalene/benzene	S/C = 1, GHSV = 19,200 h^{-1}, T = 1073 K	46	Furusawa et al. (2013)
Pt/TiO_2	1	imp	Naphthalene/benzene	S/C = 1, GHSV = 19,200 h^{-1}, T = 1073 K	20	Furusawa et al. (2013)
Ni/CeO_2	20	imp	Naphthalene/benzene	S/C = 1, GHSV = 19,200 h^{-1}, T = 1073 K	27	Furusawa et al. (2013)
Ni/ZrO_2	20	imp	Naphthalene/benzene	S/C = 1, GHSV = 19,200 h^{-1}, T = 1073 K	0	Furusawa et al. (2013)
Ni/MgO	20	imp	Naphthalene/benzene	S/C = 1, GHSV = 19,200 h^{-1}, T = 1073 K	44	Furusawa et al. (2013)
Ni/Al_2O_3	20	imp	Naphthalene/benzene	S/C = 1, GHSV = 19,200 h^{-1}, T = 1073 K	49.8	Furusawa et al. (2013)
Ni/TiO_2	20	imp	Naphthalene/benzene	S/C = 1, GHSV = 19,200 h^{-1}, T = 1073 K	23.9	Furusawa et al. (2013)
Co/MgO	20	imp	Naphthalene/benzene	S/C = 1, GHSV = 19,200 h^{-1}, T = 1073 K	23.1	Furusawa et al. (2013)
Co/MgO	12	imp	Naphthalene	S/C = 0.6, GHSV = 3,000 h^{-1}, T = 1173 K	23.3	Furusawa and Tsutsumi (2005b)
Ni/MgO	12	imp	Naphthalene	S/C = 0.6, GHSV = 3,000 h^{-1}, T = 973 K	9.4	Furusawa and Tsutsumi (2005b)
Ni/olivine	5	TI	Naphthalene	S/C = 40, GHSV = 1,166 h^{-1}, T = 1073 K	⩾98	Zhao et al. (2009)
$Ni/Ce_{0.75}Zr_{0.25-x}Mn_xO_2$	15	iw	Naphthalene	S/C = 2, GHSV = 20,000 h^{-1}, T = 973 K	100	Bampenrat et al. (2010)

[a] iw: incipient wetness method, imp: impregnation method, TI: thermal impregnation method.

low temperature and of first-order at high temperature, demonstrating that the SR of toluene over Ni/perovskite proceeded with redox mechanism using lattice oxygen of perovskite at high temperature, and Langmuir–Hinshelwood mechanism at low temperature. This change of the rate determining step was attributed to the contribution of lattice oxygen to the reaction.

It was reported by Mukai et al. that the addition of Pt to $Ni/La_{0.7}Sr_{0.3}AlO_{3-\delta}$ enhanced the activity and coke resistance for SR of toluene even without pre-reduction treatment (Mukai et al., 2014). An adjacent or alloyed structure between Pt and Ni was formed on $Pt/Ni/La_{0.7}Sr_{0.3}AlO_{3-\delta}$. Dilution effect of Pt on surface Ni and the contact between Ni and $La_{0.7}Sr_{0.3}AlO_{3-\delta}$ support were thought to be responsible for low coke deposition on $Pt/Ni/La_{0.7}Sr_{0.3}AlO_{3-\delta}$. Ni on $Pt/Ni/La_{0.7}Sr_{0.3}AlO_{3-\delta}$ was partially reduced in the reaction atmosphere without pre-reduction. This behavior was related to the improved reducibility of Ni by the addition of Pt. The additive effect of noble metals to Ni catalysts have been investigated in the methane reforming, and the addition of noble metals improves the catalytic performance in terms of activity, the suppression of coke formation, the resistance to the oxidation of Ni species (Li et al., 2011a).

Oemar et al. also reported a perovskite $LaNi_xFe_{1-x}O_3$ catalyst prepared by citric acid sol–gel method for SR of toluene (Oemar et al., 2013). The $LaNi_{0.8}Fe_{0.2}O_3$ catalyst showed the best performance in terms of activity and stability. The catalyst characterization indicated the presence of Ni-rich Ni–Fe small bimetallic particles, strong metal-support interaction, and low carbon deposition rate on $LaNi_{0.8}Fe_{0.2}O_3$. The synergy between Ni and Fe atoms on the small Ni–Fe bimetallic particles was considered to be crucial for high activity, and the strong interaction between metal and support might prevent metal aggregation, leading to high catalytic stability. Subsequently, they also found the promoting effect of Sr substitution to $LaNi_{0.8}Fe_{0.2}O_3$ (Oemar et al., 2014).

Ashok and Kawi also reported an iron–alumina-supported nickel–iron alloy catalyst for SR of toluene (Ashok and Kawi, 2013). It was found that Ni supported on an Fe_2O_3–Al_2O_3 support calcined at 773 K gave superior catalytic performance in terms of activity and stability. The catalyst gave a toluene conversion of more than 90% for a period of 26 h. According to XRD analysis, Ni–Fe alloys were formed and stable throughout the reforming reaction. The surface Fe species played the role of cocatalysts by increasing the coverage of oxygen species during the reforming reaction to enhance the reaction of toluene and suppress coke formation. TPO study on the spent catalyst revealed a low-temperature oxidation peak at around 798 K attributable to combustion of amorphous carbon. The presence of low-temperature oxidation peak for the catalyst was thought to be one of the reasons for its stable catalytic performance.

Koike et al. also reported a high-performance Ni–Fe alloy catalyst prepared from hydrotalcite-like compounds for SR of toluene (Koike et al., 2012). It was reported that uniform Ni–Fe alloy particles with an average size of 9.5 nm were formed by calcination and reduction of Ni–Mg–Fe–Al hydrotalcite-like precursor. The Ni–Fe/Mg/Al catalysts showed much higher activity than Ni/Mg/Al as well as Ni/α-Al_2O_3 and Ni–Fe/α-Al_2O_3 prepared by impregnation method. The highest activity was obtained on Ni–Fe/Mg/Al (Fe/Ni = 0.25). Moreover, the Ni–Fe/Mg/Al catalyst showed higher stability than Ni/Mg/Al. The characterization of the spent catalyst revealed a constant particle size and negligible carbon formation for Ni–Fe/Mg/Al, while the aggregation of Ni metal particles and carbon formation were clearly observed for Ni/Mg/Al. The high performance of Ni–Fe/Mg/Al catalyst was related to the nanocomposite structure consisted of uniform Ni–Fe alloy nanoparticles and Mg(Ni, Fe, Al)O nanoparticles. Uniform Ni–Fe alloy nanoparticles contributed to the high activity and coke-resistance, whereas Mg(Ni, Fe, Al)O particles located between the particles had strong

Table 3
Steam reforming of phenol over supported metal catalysts.

Catalyst	Metal loading (wt%)	Preparation method[a]	Model compound	Reaction conditions	Conversion (%)	Refs.
Rh/SiO_2	1.5	imp	Phenol	S/C = 13.3, GHSV = 80,000 h^{-1}, T = 973 K	76.0	Polychronopoulou et al. (2004a)
$Rh–CeO_2/SiO_2$	1.5	imp	Phenol	S/C = 13.3, GHSV = 80,000 h^{-1}, T = 973 K	87.3	Polychronopoulou et al. (2004a)
$Rh–ZrO_2/SiO_2$	1.5	imp	Phenol	S/C = 13.3, GHSV = 80,000 h^{-1}, T = 973 K	87.4	Polychronopoulou et al. (2004a)
Rh/ZrO_2	1.5	imp	Phenol	S/C = 13.3, GHSV = 80,000 h^{-1}, T = 973 K	82.2	Polychronopoulou et al. (2004a)
$Rh–CeO_2/ZrO_2$	1.5	imp	Phenol	S/C = 13.3, GHSV = 80,000 h^{-1}, T = 973 K	80.3	Polychronopoulou et al. (2004a)
Rh/CeO_2	1.5	imp	Phenol	S/C = 13.3, GHSV = 80,000 h^{-1}, T = 973 K	99.9	Polychronopoulou et al. (2004a)
$Rh–ZrO_2/CeO_2$	1.5	imp	Phenol	S/C = 13.3, GHSV = 80,000 h^{-1}, T = 973 K	86.0	Polychronopoulou et al. (2004a)
Rh/Ce–Zr–O	1.5	imp/sol–gel	Phenol	S/C = 13.3, GHSV = 80,000 h^{-1}, T = 973 K	84.9	Polychronopoulou et al. (2004a)
Rh/MgO	0.5	iw/sol–gel	Phenol	S/C = 13.3, GHSV = 80,000 h^{-1}, T = 973 K	88.5	Polychronopoulou et al. (2004b)
Rh/CeO_2	0.5	iw/sol–gel	Phenol	S/C = 13.3, GHSV = 80,000 h^{-1}, T = 973 K	88.3	Polychronopoulou et al. (2004b)
Rh/ZrO_2	0.5	iw/sol–gel	Phenol	S/C = 13.3, GHSV = 80,000 h^{-1}, T = 973 K	90.3	Polychronopoulou et al. (2004b)
Rh/Mg–Ce–O	0.5	iw/sol–gel	Phenol	S/C = 13.3, GHSV = 80,000 h^{-1}, T = 973 K	70.7	Polychronopoulou et al. (2004b)
Rh/Mg–Zr–O	0.5	iw/sol–gel	Phenol	S/C = 13.3, GHSV = 80,000 h^{-1}, T = 973 K	71.2	Polychronopoulou et al. (2004b)
Rh/Mg–Ce–Zr–O	0.5	iw/sol–gel	Phenol	S/C = 13.3, GHSV = 80,000 h^{-1}, T = 973 K	97.0	Polychronopoulou et al. (2004b)
Rh/Mg–Ce–Zr–O	0.1	iw/sol–gel	Phenol	S/C = 13.3, GHSV = 80,000 h^{-1}, T = 973 K	–	Polychronopoulou et al. (2012)
Rh/Mg–Ce–Zr–La–O	0.1	iw/sol–gel	Phenol	S/C = 13.3, GHSV = 80,000 h^{-1}, T = 973 K	–	Polychronopoulou et al. (2012)
Rh/Mg–Ce–Zr–Sr–O	0.1	iw/sol–gel	Phenol	S/C = 13.3, GHSV = 80,000 h^{-1}, T = 973 K	–	Polychronopoulou et al. (2012)
Rh/Mg–Ce–Zr–Zn–O	0.1	iw/sol–gel	Phenol	S/C = 13.3, GHSV = 80,000 h^{-1}, T = 973 K	–	Polychronopoulou et al. (2012)
Rh/Mg–Ce–Zr–Ca–O	0.1	iw/sol–gel	Phenol	S/C = 13.3, GHSV = 80,000 h^{-1}, T = 973 K	–	Polychronopoulou et al. (2012)
Rh/Mg–Ce–Zr–Ba–O	0.1	iw/sol–gel	Phenol	S/C = 13.3, GHSV = 80,000 h^{-1}, T = 973 K	–	Polychronopoulou et al. (2012)
$Rh/Ce_{0.15}Zr_{0.85}O_2$	0.5	iw/sol–gel	Phenol	S/C = 13.3, GHSV = 80,000 h^{-1}, T = 973 K	~55	Constantinou and Efstathiou (2010)
$Rh/Ce_{0.14}Zr_{0.81}Mg_{0.05}O_2$	0.5	iw/cp	Phenol	S/C = 13.3, GHSV = 54,000 h^{-1}, T = 723 K	~80	Constantinou and Efstathiou (2010)
$Rh/Ce_{0.13}Zr_{0.83}La_{0.06}O_2$	0.5	iw/cp	Phenol	S/C = 13.3, GHSV = 54,000 h^{-1}, T = 723 K	~77	Constantinou et al. (2012)
$Fe/MgO–CeO_2$	5	iw/sol–gel	Phenol	S/C = 13.3, GHSV = 80,000 h^{-1}, T = 923 K	63.3	Polychronopoulou et al. (2006)
$Fe/MgO/\gamma\text{-}Al_2O_3$	5	iw/iw	Phenol	S/C = 13.3, GHSV = 80,000 h^{-1}, T = 923 K	35.2	Polychronopoulou et al. (2006)
$Fe/CeO_2/\gamma\text{-}Al_2O_3$	5	iw/iw	Phenol	S/C = 13.3, GHSV = 80,000 h^{-1}, T = 923 K	61	Polychronopoulou et al. (2006)
Fe/Al_2O_3	5	iw	Phenol	S/C = 13.3, GHSV = 80,000 h^{-1}, T = 923 K	48.2	Polychronopoulou et al. (2006)
$Ni/K_2O–La_2O_3–ZrO_2$	3.5	imp/imp	Phenol	S/C = 20, GHSV = 950,000 h^{-1}, T = 973 K	85	Matas Güell et al. (2011)
$Ni/CeO_2–ZrO_2$	3.5	imp/imp	Phenol	S/C = 20, GHSV = 950,000 h^{-1}, T = 973 K	80	Matas Güell et al. (2011)
Ni–Fe/Mg/Al	12	cp	Phenol	S/C = 1.9, W/F = 0.05 g h mol^{-1}, T = 873 K	70.9	Koike et al. (2012)
Ni/Mg/Al	12	cp	Phenol	S/C = 1.9, W/F = 0.05 g h mol^{-1}, T = 873 K	47.4	Koike et al. (2012)
$Ni/\alpha\text{-}Al_2O_3$	12	iw	Phenol	S/C = 1.9, W/F = 0.05 g h mol^{-1}, T = 873 K	19.2	Koike et al. (2012)
$Ni–Fe/\alpha\text{-}Al_2O_3$	12	iw	Phenol	S/C = 1.9, W/F = 0.05 g h mol^{-1}, T = 873 K	11.2	Koike et al. (2012)

[a] iw: incipient wetness method, imp: impregnation method, cp: co-precipitation method.

interaction with the particles and could suppress the aggregation of particles.

SR of toluene was also conducted on Ni–Co/α-Al_2O_3, Ni/α-Al_2O_3, and Co/α-Al_2O_3 catalysts by Wang et al. (2013). The order of activity, stability, and coke-resistance in SR of toluene was found to be Co/α-Al_2O_3 > Ni–Co/α-Al_2O_3 > Ni/α-Al_2O_3. SR of toluene over Co–Fe/α-Al_2O_3 catalyst was also conducted by Koike et al. (2013a) and Wang et al. (2012). Interestingly, in the SR of toluene without the presence of H_2, Co–Fe/α-Al_2O_3 showed a higher initial activity than Co/α-Al_2O_3, however, it was deactivated quickly, giving lower steady-state activity than Co/α-Al_2O_3. By the addition of H_2 to SR of toluene, the catalytic stability of Co–Fe/α-Al_2O_3 was enhanced remarkably, leading to higher steady-state activity than that of Co/α-Al_2O_3. The XRD characterization of the spent catalysts revealed that the bcc Co–Fe alloys disappeared without the presence of H_2, which could be attributed to the oxidation of bcc Co–Fe alloys by steam. On the other hand, the oxidation of bcc Co–Fe alloys was effectively suppressed by the addition of H_2 and this might be related to the strong adsorption of H_2 on the bcc Co–Fe alloy surface. It was considered that the bcc Co–Fe alloy phase was responsible for the high activity in the SR of toluene. The reaction kinetics study of SR of toluene in the presence of H_2 over the Co–Fe/α-Al_2O_3 catalyst showed first and negative reaction order with respect to toluene and steam. It was considered that the activation of toluene was an important elementary step and might proceed at the methyl group. Based on these results, it was concluded that the high activity of Co–Fe/α-Al_2O_3 in the SR of toluene with the presence of hydrogen might be caused by the synergy over bcc Co–Fe alloy surface. The presence of hydrogen could suppress the oxidation of Fe species on the Co–Fe alloy phase with steam. The metallic surface of the bcc Co–Fe alloy had a strong interaction with hydrogen and the coverage of adsorbed hydrogen species could be maintained to be high. The hydrogen species might also help the activation of toluene via its methyl group (Koike et al., 2013a).

Li et al. developed a nickel-based mayenite catalyst (Ni/$Ca_{12}Al_{14}O_{33}$) by solid mixing method (Li et al., 2009). The Ni/$Ca_{12}Al_{14}O_{33}$ catalyst was reported to show excellent sustainability against coke deposition. The catalyst also exhibited higher H_2S-poisoning resistance property than Ni/Al_2O_3 and Ni/$CaO_{0.5}$/$MgO_{0.5}$. Raman spectra revealed that "free oxygen O_2^- and O_2^{2-}" in the structure of the catalysts could be substituted by sulfur then protected Ni poisoning on some degree. Nevertheless, the sulfide Ni/$Ca_{12}Al_{14}O_{33}$ was difficult to completely restore by O_2 and H_2 treatment at 923 K, and the sulfur in the mayenite structure was only partially re-substituted with O_2.

Quitete et al. evaluated the activity and coke resistance of Ni catalysts supported on hexaaluminates in SR of toluene (Quitete et al., 2014). There existed a linear relationship between the coking rates and the Ni particle sizes. Catalysts with lower nickel dispersion exhibited lower initial toluene conversion at 923 K. The initial activity order was Ni/$CaAl_{12}O_{19}$ > Ni/$La_{0.8}Ce_{0.2}Al_{11}O_{19}$ > Ni/$LaAl_{11}O_{18}$ with 6 wt% Ni. The amount of coke formation did not follow the order of deactivation during reaction; on the other hand, the catalysts with higher deactivation rates presented severe Ni sintering. Ni/$La_{0.8}Ce_{0.2}Al_{11}O_{19}$ showed higher stability during 16 h of toluene SR than Ni/$LaAl_{11}O_{18}$ and Ni/$CaAl_{12}O_{19}$, which was coherent with its higher resistance to coke deposition.

Koike et al. reported that the addition of MnO_x oxide to Ni/α-Al_2O_3 improved the activity and stability in the SR of toluene at 873 K (Koike et al., 2013b). Also, the MnO_x addition enhanced the resistance to coke deposition, which was related to higher stability of Ni + MnO_x/α-Al_2O_3. The promoting effect of MnO_x addition might be explained by the cocatalysis of MnO_x due to its high redox property. It was suggested that the surface of Ni metal particles was partially covered with MnO_x species, and the oxygen atoms derived from MnO_x species could be supplied to the Ni species to promote the reaction between carbonaceous species on Ni and oxygen species.

2.2. Steam reforming of naphthalene over metal catalysts

It has been well-known that SR of naphthalene is more difficult than that of benzene and toluene. It was reported (Coll et al., 2001) that the order of reactivity of tar model compounds in SR on a commercial Ni catalyst was benzene > toluene ≫ anthracene ≫ pyrene > naphthalene. The tendency towards coke formation was found to increase with increasing the molecular weight of the aromatic compounds. This can be because the reforming rate becomes lower as the molecular weight increased, and the structure became more similar to that of coke as the number of aromatic rings increased.

Furusawa et al. investigated the influence of support on the performances of Pt and Ni catalysts for the SR of naphthalene/benzene (Furusawa et al., 2013). In the case of Pt catalysts, the activity order was Pt/MgO > Pt/Al_2O_3 > Pt/CeO_2, Pt/TiO_2 ≫ Pt/ZrO_2. The high activity of Pt/MgO was related to its small Pt particle size resulting from the strong interaction between Pt precursor and MgO support, and the low activity of Pt/CeO_2 and Pt/TiO_2 was explained by the loss of Pt metal active sites caused by partial coverage of reduced CeO_x or TiO_x on the Pt metal particles due to strong metal-support interaction (SMSI). However, the Pt/Al_2O_3 catalyst was deactivated at 1023 K due to the aggregation of Pt metal particles, and the Pt/MgO catalyst lost its activity quickly at 1073 K and S/C = 3, which was attributed to the size increase and morphology change of MgO support under the high concentration of steam atmosphere. In the case of Ni catalysts, the activity order was Ni/Al_2O_3 > Ni/MgO > Ni/CeO_2 > Ni/TiO_2 ≫ Ni/ZrO_2. The Ni/Al_2O_3 catalyst showed stable activity for 30 h at 1073 K, while the Ni/MgO catalyst was deactivated due to the oxidation of Ni metal and the size increase of MgO support. The effect of regeneration method on the catalytic performance of Pt/Al_2O_3 and Ni/Al_2O_3 catalysts was also investigated and it was found that hydrogen treatment was better regeneration method than oxygen treatment, the latter causing the aggregation of metal particles and/or the formation of inactive phase.

Ozkan and coworkers prepared a Ni–olivine catalyst by thermal impregnation (TI) method and tested the catalytic performance in SR of naphthalene (Kuhn et al., 2008; Zhao et al., 2008, 2009). In the thermal impregnation, Ni precursor such as metallic Ni or NiO was integrated into the olivine structure by heating under an Ar atmosphere at higher temperatures like 1673 K. The Ni–olivine catalyst prepared by TI showed much higher activity compared to the olivine support, giving ⩾98% conversion of naphthalene at 1073 K. Additionally, the Ni–olivine catalyst prepared by TI showed similar high-temperature activity and lower coke deposition rates compared to that prepared by incipient wet impregnation. Stronger interactions between Ni and the olivine support for the TI catalyst were proposed to account for the improved catalytic properties. The suppression of coke deposition was explained as due to the formation of (Mg, Ni)O and/or a Ni–Fe alloy.

Bampenrat et al. investigated the SR of naphthalene over Mn-doped CeO_2–ZrO_2 supported Ni catalysts (Bampenrat et al., 2010). The Ni/$Ce_{0.75}Zr_{0.25-x}Mn_xO_2$ mixed oxide catalysts exhibited high activities and stabilities. It was found that the amount of carbon deposition became smaller when Mn was introduced to the CeO_2–ZrO_2 mixed oxide. This might be explained by that the incorporation of manganese ions into the ceria lattice improved the oxygen storage capacity and the oxygen mobility on the surface of mixed oxides, resulting in enhancing the gasification of the deposited carbon.

SR of naphthalene over Co supported catalysts was investigated by Furusawa and Tsutsumi (2005b). It was found that the Co/MgO catalyst with 12 wt% Co and calcined at 873 K showed the best catalytic performance after reduction at 1173 K. This good performance was related to the high amount of Co metal surface atoms and the small amount of coke deposition on the catalyst. The Co/MgO catalyst was found to show higher activity than Ni/MgO catalyst (Furusawa and Tsutsumi, 2005a). It was pointed out that the SR of naphthalene proceeded in stoichiometric ratio between the carbon atoms of naphthalene and H_2O over Co catalyst; however, the activation of excess H_2O happened over Ni catalyst, which led to its lower activity than Co catalyst.

In recent years, Baron and coworkers have developed a novel Ni-activated ceramic candle filter for hot biomass gasification gas, where particle removal and tar reforming were integrated in one process unit (Draelants et al., 2001; Engelen et al., 2003; Ma et al., 2005; Zhao et al., 2000a,b). The catalytic filter consisted of a ceramic α-Al_2O_3 porous filter substrate in which a catalytically active nickel-based catalyst was deposited onto the pore walls to convert the tars. To incorporate the Ni catalyst in the filter, deposition–precipitation with urea was adopted. It was reported that a porous alumina filter containing ~1.2 wt% ZrO_2, 1.3 wt% Al_2O_3, 1.0 wt% Ni and 0.5 wt% MgO showed good performance (Ma and Baron, 2008). At 900 °C and a typical face velocity of 2.5 cm s^{-1}, in the presence of 100 ppm H_2S, the conversions of benzene and naphthalene were 95% and 99.5%, respectively. At a long-term testing over 170 h, the catalytic candle filter showed 99.2–99.6% benzene conversion and 100% naphthalene conversion. Except for the development of a catalytic coating on the porous support, other ways to integrate a catalyst in a ceramic filter was also reported, such as the integration of a catalyst particle layer or catalytic ceramic foam (Nacken et al., 2007, 2012). It was reported that an Al_2O_3 based catalytic filter candle with integrated catalytic ceramic foam showed 98% conversion of naphthalene at 850 °C in the presence of 100 ppm H_2S. It seems that this kind of catalytic candle filter is technically feasible for efficient tar reforming. One of the advantages of integrating the catalyst in the filter is that it simplifies the entire gas cleaning process and could bring about a reduction in investment costs. Another major advantage is the elimination of the internal mass transfer resistance occurring in the packed or fluidized catalyst bed. From the economic and technical point of view, this kind of structured catalyst appears attractive for hot biomass gasification gas cleaning.

2.3. Steam reforming of phenol over metal catalysts

Efstathiou and coworkers conducted many works on the SR of phenol over metal catalysts. It was reported that the support composition significantly influenced the catalytic activity and selectivity of the SR of phenol towards H_2 formation over supported Rh catalysts. Among the supports of CeO_2, ZrO_2, SiO_2, CeO_2/SiO_2, ZrO_2/SiO_2, ZrO_2/CeO_2, and CeO_2/ZrO_2, the Rh–ZrO_2/SiO_2 and Rh–CeO_2/SiO_2 catalysts presented higher H_2 product, while Rh/SiO_2 was the worst (Polychronopoulou et al., 2004a). The high activity of Rh–ZrO_2/SiO_2 and Rh–CeO_2/SiO_2 was attributed to the presence of ZrO_2 and CeO_2, which might promote the water–gas shift reaction and/or supply active oxygen species to the Rh surface to keep Rh surface free of carbon residues. It was also found that the Rh/Ce–Zr–O catalyst, the support of which was prepared by the sol–gel method, exhibited better performance than those CeO_2/ZrO_2 and ZrO_2/CeO_2 supported catalysts and a commercial Ni-based catalyst. The high performance of Rh/Ce–Zr–O was due to the presence of small Rh particles and the formation of $Ce_xZr_{1-x}O_2$ solid solution that presented better thermal stability, higher oxygen storage capacity (OSC), and a larger amount of easily reducible oxygen species than both pure CeO_2 and ZrO_2. The catalyst showed also no more than 18% drop in activity after 24 h of continuous reaction.

In another study, Efstathiou and coworkers investigated the SR of phenol over various MgO-based supported Rh catalysts (Polychronopoulou et al., 2004b). It was found that 0.5 wt% Rh/MgO and 0.1 wt% Rh/Mg–Ce–Zr–O catalysts exhibited better performance than those supported on ZrO_2, CeO_2, Mg–Ce–O, and Mg–Zr–O. SR of phenol was favored over very small Rh particles in the case of 0.1 wt% Rh/Mg–Ce–Zr–O catalyst. In particular, the specific integral reaction rate of H_2 production significantly increased by decreasing the Rh particle size from 2.7 to 1.2 nm. XPS studies suggested that the $Mg_xZr_{1-x}O_2$ phase presented in the Mg–Ce–Zr–O support was reduced by H_2 at 573 K in the presence of very small Rh particles leading to the creation of oxygen vacant sites and diffusion of Zr toward the bulk of crystal. As a result of this, the surface acidity and basicity of the Rh/Mg–Ce–Zr–O catalyst were expected to alter, thus influencing the hydrogen activity and selectivity of the reaction.

The addition of alkaline-earth, rare earth metal oxides, and transition metal oxides (La, Sr, Ba, Ca, Zn) on the performance of Rh/Mg–Ce–Zr–O was further investigated (Polychronopoulou et al., 2012). The 0.1 wt% Rh/Mg–Ce–Zr–La–O catalyst was found to exhibit the highest hydrogen product yield, specific H_2 production rate and the lowest CO/CO_2 product ratio. This behavior was correlated with the largest concentration of basic sites and labile oxygen species, and also with the largest acid/base site ratio present in the Mg–Ce–Zr–La–O support composition.

Efstathiou and coworkers investigated the SR of phenol in the low temperature range of 623–823 K over 0.5 wt% Rh supported on $Ce_{0.15}Zr_{0.85}O_2$, $Zr_{0.93}La_{0.07}O_2$, and $Ce_{0.13}Zr_{0.83}La_{0.04}O_2$ mixed oxides (Constantinou et al., 2012). It was found that the reforming specific activity (per gram of catalyst basis) was dependent on Rh dispersion, the concentration of labile oxygen species of support, and the promotion of the water–gas shift reaction rate, all of which largely influenced by the support chemical composition. The addition of 4 at.% La^{3+} into the $Ce_{0.15}Zr_{0.85}O_2$ was found to largely promote the dispersion of Rh, to increase significantly the concentration of surface basic sites of $Ce_{0.13}Zr_{0.83}La_{0.04}O_2$ compared to $Ce_{0.15}Zr_{0.85}O_2$ support, to prevent to a large extent the inhibiting role of hydrogen in the rate of WGS reaction, and to influence significantly the concentration and structure of surface reaction intermediates of the WGS, namely: formate (HCOO–) and –OH groups formed on the support and adsorbed CO formed on the Rh metal. The 0.5 wt% Rh/$Ce_{0.13}Zr_{0.83}La_{0.04}O_2$ catalyst showed a significantly better performance towards SR of phenol in terms of phenol conversion, H_2-yield, and CO/CO_2 product ratio compared to a commercial Ni-based catalyst (44 wt% Ni). Similar promoting effect of Mg addition to Rh/$Ce_{0.15}Zr_{0.85}O_2$ was reported (Constantinou and Efstathiou, 2010).

Supported Fe catalysts have also been investigated for SR of phenol by Efstathiou and coworkers (Polychronopoulou et al., 2006). Among the supports of MgO–CeO_2, MgO/γ-Al_2O_3, CeO_2/γ-Al_2O_3, and γ-Al_2O_3, the 50 at.% MgO–50 at.% CeO_2 support prepared by sol–gel method was the most suitable. For supported Fe/MgO–CeO_2 catalysts, the optimum loading of Fe was 5 wt%. The 5 wt% Fe/MgO–CeO_2 catalyst showed the highest performance in terms of phenol conversion and H_2 yield. The 5 wt% Fe/MgO–CeO_2 catalyst also showed a good stability under consecutive oxidation → reaction → oxidation → reduction → reaction cycles. Mössbauer studies revealed that Fe was present as Fe^{2+} and Fe^{3+} during phenol SR and a high Fe^{2+}/Fe^{3+} ratio was present on the most active 5 wt% Fe/MgO–CeO_2 catalyst. A bifunctional catalysis was proposed for the SR of phenol on the Fe/MgO–CeO_2 catalyst. Phenol is adsorbed dissociatively on the iron oxide surface to form surface phenoxy species. The derived hydrocarbon fragments from the phenoxy adsorbed species are oxidized by labile O and/or –OH species of

support via a back-spillover process, and by –OH groups residing on iron oxide surface to form H_2, CO, and CO_2.

Matas Güell et al. examined the influence of support on the catalytic performances for SR of phenol over Ni/K–La–ZrO_2 and Ni/Ce–ZrO_2 (Matas Güell et al., 2011). Compared to Ni/CeO_2–ZrO_2, Ni/K–La–ZrO_2 showed a substantial change in gas product distribution with time on stream, during which H_2 and CO_2 yields decreased and CO yield increased. This was attributed to the deactivation for the water–gas shift caused by the coke deposition on the active Ni surface. It was observed that coke deposits on Ni/K–La–ZrO_2 accumulated mainly on the Ni surface, while coke on Ni/CeO_2–ZrO_2 was evenly distributed over the Ni metal and support surface. The difference in the location of carbonaceous deposits was related to the redox property of supports. It was thought that the high redox property of CeO_2–ZrO_2 support could result in more oxygenated species (O^- and OH^-), which might undergo back-spillover from the support to the Ni metal surface, promoting the gasification of the carbonaceous species accumulated on Ni and keeping the Ni surface clean for water–gas shift.

SR of phenol over Ni–Fe/Mg/Al alloy catalyst prepared from hydrotalcite-like compounds was also investigated by Koike et al. (2012). The activity of Ni–Fe/Mg/Al was much higher than those of Ni/Mg/Al as well as Ni/α-Al_2O_3 and Ni–Fe/α-Al_2O_3 prepared by conventional impregnation method. It was found that the promoting effect of Fe on the hydrotalcite-derived catalysts was more significant than on Al_2O_3-supported catalysts, and this was attributed to the uniformity of the Ni–Fe alloy nanoparticles.

3. Catalyst development using biomass-derived tar

Development of metal catalysts for SR of biomass tar has been conducted by several research groups. Li et al. (2008) prepared a supported nano-NiO/γ-Al_2O_3 catalyst by deposition–precipitation method. The prepared nano-NiO/γ-Al_2O_3 catalyst had a coated structure and a higher BET surface area (111.8 $m^2\ g_{cat}^{-1}$) over commercial nickel based catalysts. The spherical NiO nanoparticles coated on the surface of supports had a size of 12–18 nm. The nano-NiO/γ-Al_2O_3 was reported to show high activity for tar removal in the process of biomass pyrolysis using a bench-scale combined fixed bed reactor. In the presence of the catalyst, the tar remove efficiency reached to 99% at 1073 K. Wang et al. reported a highly stable NiO–MgO catalyst prepared by co-precipitation method (Wang et al., 2006). The NiO–MgO catalyst exhibited excellent reducibility and highly stable activity for the reforming of raw fuel gas without pre-reduction. No deactivation and very little carbon deposition were observed during 100 h lifetime test. The highly stable activity was attributed to the small Ni particle size, high dispersion of Ni particles in the NiO–MgO solid solution structure, and the promotion by catalyst reducibility. Corujo et al. reported that the use of NiO-loaded calcined dolomite catalysts led to a reduction in the formation rate of tar and char and a 30% increase in the total product gas (Corujo et al., 2010). In addition, Xiao et al. (2011) and Wang et al. (2011a) reported the preparation of char-supported Ni catalysts that were shown to be effective for SR of tar.

Further catalyst development has been carried out in various ways, and here two typical aspects in the development are introduced.

3.1. Metal catalysts supported on conventional oxides for steam reforming of biomass tar

A previous study of SR of biomass tar over Ni catalysts supported on α-Al_2O_3, ZrO_2, TiO_2, CeO_2, and MgO (Miyazawa et al., 2006) revealed that Ni/α-Al_2O_3 had higher activity than the other supported catalysts (see Table 4). The activity order was Ni/α-Al_2O_3 > Ni/ZrO_2 > Ni/TiO_2 > Ni/CeO_2 > Ni/MgO in terms of residual tar yield. Nevertheless, the Ni/α-Al_2O_3 catalyst suffered from a large amount of coke deposition. On the other hand, the coke deposition on the Ni/CeO_2 catalyst was relatively small. This was properly due to the high redox property of Ce species. To improve the performance of Ni/α-Al_2O_3 catalyst, the additive effect of CeO_2 was investigated (Kimura et al., 2006; Tomishige et al., 2007). It was found that the Ni/CeO_2/α-Al_2O_3 catalyst prepared by the co-impregnation method exhibited higher performance than Ni/α-Al_2O_3 and Ni/CeO_2/α-Al_2O_3 prepared by the sequential impregnation method. The characterization results suggested that the interaction between Ni and CeO_2 became stronger by the co-impregnation method than that by sequential method and that Ni–CeO_2 nanocomposite was formed. The carbonaceous reaction intermediate species adsorbed

Table 4
Steam reforming of biomass tar over metal catalysts reported in our group.

Catalyst	Metal loading (wt%)	Preparation method[a]	Catalyst loading (g)	S/C	Tar yield (%)	Coke yield (%)	Formation rate of ($CO + H_2 + 4CH_4$) (μmol min^{-1})	Refs.
Ni/α-Al_2O_3	12	iw	1	0.50	9.3	12.7	2352	Miyazawa et al. (2006)
Ni/ZrO_2	12	iw	1	0.50	12.4	6.6	2217	Miyazawa et al. (2006)
Ni/TiO_2	12	iw	1	0.50	12.9	15.1	2142	Miyazawa et al. (2006)
Ni/CeO_2	12	iw	1	0.50	25.7	4.3	1830	Miyazawa et al. (2006)
Ni/MgO	12	iw	1	0.50	28.6	10.4	1554	Miyazawa et al. (2006)
Ni/CeO_2/α-Al_2O_3	4	iw	1	0.50	3.6	8.6	2949	Kimura et al. (2006)
Pt–Ni/CeO_2/α-Al_2O_3	4	iw	1	0.50	0	6.5	3103	Nishikawa et al. (2008b)
Pt–Ni/CeO_2/MgO/α-Al_2O_3	12	iw	1	0.47	1.6	8.0	3445	Nakamura et al. (2009)
Ni + MnO_x/α-Al_2O_3	12	iw	0.5	0.47	0	5.6	3214	Koike et al. (2013a,b)
Ni–Fe/α-Al_2O_3 (Fe/Ni = 0.5)	12	iw	0.75	0.47	6.2	9.2	2864	Wang et al. (2011b)
Ni–Co/α-Al_2O_3 (Co/Ni = 0.25)	12	iw	0.75	0.47	3.8	6.2	3091	Wang et al. (2013)
Co–Fe/α-Al_2O_3 (Fe/Ni = 0.25)	12	iw	0.75	0.47	0	5.0	3415	Wang et al. (2012)
Co/α-Al_2O_3	12	iw	0.75	0.47	5.5	11.6	2766	Li et al. (2013)
Co/$BaAl_{12}O_{19}$	12	iw	0.75	0.47	0	13.0	3050	Li et al. (2013)
Ni/Mg/Al	12	cp	0.3	0.47	0	8.4	3279	Li et al. (2011a,b)
Co/Mg/Al	12	cp	0.3	0.47	0	6.7	2449	Wang et al. (2014b)
Ni–Fe/Mg/Al (Fe/Ni = 0.25)	12	cp	0.3	0.38	0	4.0	3594	Li et al. (2014b)
Ni–Cu/Mg/Al (Cu/Ni = 0.25)	12	cp	0.3	0.38	0	3.1	3683	Li et al. (2014a)
Co–Fe/Mg/Al (Co/Ni = 0.25)	12	cp	0.3	0.38	0	5.2	2655	Wang et al. (2014a)

Other reaction conditions: cedar, 60 mg min^{-1} (C = 2360 μmol min^{-1}, H = 3350 μmol min^{-1}, O = 1450 μmol min^{-1}); T = 823 K.
[a] iw: incipient wetness method, cp: co-precipitation (via hydrotalcite-like compounds).

on Ni metal surface can react with oxygen atom supplied from neighboring CeO_2, resulting in high catalytic activity and low coke deposition.

The catalytic performance of $Ni/CeO_2/\alpha$-Al_2O_3 was further improved by the modification with a small amount (~0.1 wt%) of noble metals (Nishikawa et al., 2008a,b). The noble metal-promoted $Ni/CeO_2/\alpha$-Al_2O_3 catalysts without H_2 reduction showed self-activation ability in the SR of tar. Among the noble metals investigated (Pd, Ru, Rh, Pt), Pt was the most effective. The high performance of $Pt/Ni/CeO_2/\alpha$-Al_2O_3 was related to the strong interaction between Pt and Ni by the formation of Pt–Ni alloy, while Rh, Ru, and Pd did not alloy with Ni, but interacted with CeO_2. However, the $Pt/Ni/CeO_2/\alpha$-Al_2O_3 catalyst was deactivated in the SR of tar within 2 h of test at 923 K due to the aggregation of Ni metal particles.

The aggregation of Ni metal particles might be effectively suppressed by the addition of MgO (Nakamura et al., 2009). It was found that the $Pt/Ni/CeO_2/MgO/\alpha$-Al_2O_3 catalyst maintained high catalytic activity even after 4 h of test, demonstrating the enhanced stability by the addition of MgO. This behavior was related to the improved dispersion of Ni metal particles resulting from the formation of NiO–MgO solid solution and high resistance to the aggregation by the strong interaction between Ni and MgO (Tomishige et al., 1999; Yamazaki et al., 1996). Another interesting property was that the aggregated Ni particles on the $Pt/Ni/CeO_2/MgO/\alpha$-Al_2O_3 catalyst became re-dispersed by the catalyst regeneration (oxidation at 873 K and reduction at 773 K). The re-dispersion might proceed via the formation of the NiO–MgO solid solution by oxidation and the subsequent reduction of the NiO–MgO. In addition, the $Pt/Ni/CeO_2/MgO/\alpha$-Al_2O_3 catalyst could be activated automatically by the reactants, showing the ability of self-activation. By the addition of Pt, CeO_2, and MgO, the $Pt/Ni/CeO_2/MgO/\alpha$-Al_2O_3 catalyst exhibited various important properties including high activity, stability, self-activation, and self-regeneration.

From the above results, it is known that the redox property of CeO_2 and the Ni–CeO_2 interface play an important role in the SR of tar. Besides CeO_2, MnO_2 is also an effective additive. Koike et al. (2013b) reported that the addition of MnO_2 to Ni/α-Al_2O_3 catalyst by co-impregnation method showed improved activity and coke-resistance in SR of tar. The highest activity was obtained on the $Ni + MnO_x/\alpha$-Al_2O_3 catalyst with 20 wt% MnO_2 addition. The activity of $Ni + MnO_x/\alpha$-Al_2O_3 was even higher than that of $Ni + CeO_2/\alpha$-Al_2O_3. In addition, the $Ni + MnO_x/\alpha$-Al_2O_3 catalyst showed higher resistance to coke deposition than the $Ni + CeO_2/\alpha$-Al_2O_3 catalyst. These results indicated that the additive effect of MnO_2 was more significant than that of CeO_2. The Ni metal surface was partially covered with MnO_x species and the promoting effect of MnO_2 addition could be explained by the redox property of MnO_x in a similar way as that of CeO_2 addition, that is, the oxygen atoms derived from MnO_x species could be supplied to the Ni species to promote the reaction between carbonaceous species on Ni and oxygen species.

Alloying of Ni metal with noble metals has demonstrated an effective approach to improve the catalytic performance. In particular, the catalyst reducibility and the coverage of oxygen atoms can be controlled by the combination of metals with different oxygen affinity. For example, the combination between Ni and other metal with lower oxygen affinity than Ni can make the alloy reducibility higher than monometallic Ni. In contrast, the combination between Ni and other metal with higher oxygen affinity than Ni can make the coverage of oxygen atoms during the reforming reaction higher than the case of monometallic Ni catalyst. Wang et al. (2011b) reported that the addition of suitable amount of Fe to Ni/α-Al_2O_3 enhanced the catalytic performance in the SR of tar. A volcano-type dependence of the activity on the amount of added Fe was observed. The highest activity was obtained on Ni–Fe/α-Al_2O_3 (Fe/Ni = 0.5), which exhibited higher activity, stability, and resistance to coke deposition than the corresponding monometallic Ni/α-Al_2O_3 and Fe/α-Al_2O_3 catalysts. Catalyst characterization indicated that fcc and bcc Ni-Fe alloys as well as tetragonal NiFe phase were formed depending on the Fe/Ni ratios. Particularly, Fe atoms tend to be located on the surface of the alloy particles. The formation of Ni–Fe alloys was also confirmed by XRD on Ni–Fe/α-Al_2O_3 (Fe/Ni = 0.5) after stability test. It was found that the tetragonal NiFe phase reduced and the fcc Ni–Fe alloys grew up with increased composition of Fe to Ni. This indicated that most Fe species were kept in a metallic state in the alloy particles during the reaction, and the oxidation of Fe species to the Fe oxide was suppressed. High performance of the Ni–Fe/α-Al_2O_3 catalyst was attributed to the synergy between the activation of tar on the Ni species and the supply of oxygen atom from neighboring Fe sites. It was suggested that the addition of Fe to Ni could increase the coverage of oxygen atoms during the SR reactions considering that Fe has higher oxygen affinity than Ni (Reed, 1971). The oxygen atoms on Fe species might be quickly supplied to the Ni species to promote the gasification of carbonaceous species on Ni surface, enhancing the reaction of tar and suppressing the coke deposition.

The promoting effect of alloying was also observed on Ni–Co/α-Al_2O_3 and Co–Fe/α-Al_2O_3 catalysts. For Ni–Co/α-Al_2O_3 (Wang et al., 2013), the optimum composition was obtained at Co/Ni = 0.25. Similarly to Ni–Fe/α-Al_2O_3 (Fe/Ni = 0.5), the Ni–Co/α-Al_2O_3 (Co/Ni = 0.25) catalyst showed the formation of Ni–Co alloys (fcc) and gave higher activity, stability, and resistance to coke deposition than the corresponding monometallic Ni/α-Al_2O_3 and Co/α-Al_2O_3 catalysts. The activity order in the SR of biomass tar was Ni–Co/α-Al_2O_3 (Co/Ni = 0.25) > Co/α-Al_2O_3 > Ni/α-Al_2O_3. On the other hand, it was Co/α-Al_2O_3 > Ni–Co/α-Al_2O_3 (Co/Ni = 0.25) > Ni/α-Al_2O_3 in the SR of toluene. The different tendency in the SR of tar and toluene was explained by the high activity of Ni–Co/α-Al_2O_3 for the SR of oxygenates due to the synergy between Ni and Co. However, further investigations on the SR of model oxygenates was necessary to elucidate the synergy between Ni and Co in the SR of tar.

For Co–Fe/α-Al_2O_3 (Wang et al., 2012), fcc and bcc Co–Fe alloys were formed depending on the Fe/Co ratios and bcc Co–Fe alloys were primarily formed at higher Fe/Co ratios. It was noted that Fe tended to give bcc alloy much preferentially on Co–Fe/α-Al_2O_3 than on Ni–Fe/α-Al_2O_3. In the SR of tar, the highest activity was obtained on Co–Fe/α-Al_2O_3 (Fe/Co = 0.25), on which both fcc and bcc Co–Fe alloys were formed. It was noted that among the alloy catalysts developed, Co–Fe/α-Al_2O_3 (Fe/Co = 0.25) showed the highest activity, followed by Ni–Co/α-Al_2O_3 (Co/Ni = 0.25) and then Ni–Fe/α-Al_2O_3 (Fe/Ni = 0.5).

As described above, Co also appears to be a promising active metal for SR of tar besides Ni. Co catalysts supported on various oxide supports were then investigated (Li et al., 2013). Barium hexaaluminates ($BaAl_{12}O_{19}$) was chosen as a support because of its high thermal stability. It was found that $Co/BaAl_{12}O_{19}$ showed higher activity in the SR of tar than those supported on α-Al_2O_3, ZrO_2, SiO_2, MgO, and TiO_2. The Co metal particles supported on $BaAl_{12}O_{19}$ had high dispersion. High dispersion of Co metal particles on $Co/BaAl_{12}O_{19}$ might account for the high activity, and the high dispersion was related to the strong basicity of the $BaAl_{12}O_{19}$ surface. Strong basicity of $BaAl_{12}O_{19}$ and high dispersion of Co metals particles were connected to high H_2O reactivity to form H_2, probably at the interface between Co metal and $BaAl_{12}O_{19}$. In addition, the $Co/BaAl_{12}O_{19}$ catalyst exhibited higher reusability through the coke combustion (873 K) and the subsequent reduction treatment (773 K) than the Co/α-Al_2O_3 catalyst. This was attributed to the suppression of the solid reaction between the oxidized Co and $BaAl_{12}O_{19}$.

In the catalyst development described above, the catalysts were prepared by the conventional impregnation method. The disadvantage of this preparation method is that it usually gave large metal particles and weak interaction between metal particles and support, leading to coke deposition and aggregation of metal particles. Especially for alloy catalysts, it might cause large inhomogeneity in the composition of the particles, leading to the formation of alloy particles with different structures such as fcc alloy, bcc alloy, and/or intermetallic compounds (Wang et al., 2011b, 2012). Since the catalytic performances of alloy particles are greatly dependent on the structure, composition, and particle size, the preparation of uniform and well-dispersed alloy particles is highly desired. In this respect, one promising approach is the use of hydrotalcite-like compounds as catalyst precursor.

3.2. Metal catalysts prepared from hydrotalcite-like compounds for steam reforming of biomass tar

Hydrotalcite-like compounds (HTlcs, $[M^{2+}_{1-x}M^{3+}_{x}(OH)_2]^{x+}(A^{n-}_{x/n})\cdot mH_2O$), are layered double hydroxide that consists of positively charged two-dimensional brucite-like sheets in which a fraction of the divalent cations are isomorphously substituted by trivalent cations, together with charge-compensating anions and water in the interlayer (Cavani et al., 1991). Upon calcination, HTlcs form mixed oxides that show several interesting properties such as high dispersion, thermal stability, large surface area, and basic character. Moreover, the mixed oxides give rise to well-dispersed and thermally stable metal particles by reduction treatments when reducible cations are present.

Recently, Li et al. reported a Ni/Mg/Al catalyst prepared from Ni–Mg–Al HTlcs for the SR of tar derived from the pyrolysis of biomass (Li et al., 2011b). Studies on the chemical compositions and reduction treatments revealed that the Ni/Mg/Al catalyst with Ni/Mg/Al = 9/66/25 and reduced at 1073 K in 50% H_2/N_2 showed good performance. The optimized Ni/Mg/Al catalyst exhibited much higher activity, resistance to coke deposition, and stability than Al_2O_3- and MgO-supported Ni catalysts. The characterization indicated that the Ni/Mg/Al catalyst after the reduction had a nanocomposite structure consisted of Ni metal particles (~8.5 nm) and Mg(Ni, Al)O particles (~11.5 nm). The formation of nanocomposite is expected to enhance the interface between Ni metal and oxide support, meanwhile it can play an important role on the suppression of the aggregation of metal particles.

By introduction of Fe into Ni–Mg–Al HTlcs, Li et al. successfully prepared a uniform Ni–Fe alloy supported catalyst from Ni–Mg–Fe–Al HTlcs (Li et al., 2014b). It was reported that only fcc Ni–Fe alloy was formed at the range of Fe/Ni = 0–1.5. For Fe/Ni $\leqslant$ 0.5, the Ni–Fe alloy particles had relatively uniform composition, as determined by EDX. It was considered that both Ni^{2+} and Fe^{3+} cations were homogenously distributed in the hydrotalcite-like precursor and highly dispersed in the Mg(Ni, Fe, Al)O calcined product, leading to the formation of uniform Ni–Fe alloy nanoparticles upon reduction. These uniform Ni–Fe alloy nanoparticles exhibited very high activity for the SR of biomass tar. The highest activity was obtained on the Ni–Fe/Mg/Al (Fe/Ni = 0.25) catalyst with the composition of Ni/Fe/Mg/Al = 9.6/2.5/65.4/22.5. The catalytic performance was significantly higher than those of Ni/Al_2O_3 catalysts modified with MnO_2, CeO_2 or alloying with Fe and Co as well as $Rh/CeO_2/SiO_2$. More importantly, the Ni–Fe/Mg/Al (Fe/Ni = 0.25) catalyst exhibited much better regenerability toward the oxidation–reduction treatment than the conventional α-Al_2O_3-supported Ni–Fe catalyst. The XRD characterization on the spent Ni–Fe/α-Al_2O_3 (Fe/Ni = 0.5) catalyst showed the aggregation and/or structural changes of alloy particles during the reaction and the regeneration treatment. On the other hand, the Ni–Fe alloy nanoparticles on Ni–Fe/Mg/Al (Fe/Ni = 0.25) could be regenerated by the oxidation–reduction treatment. It was considered that the Ni–Fe alloy nanoparticles on Ni–Fe/Mg/Al (Fe/Ni = 0.25) were oxidized to Ni^{2+} and Fe^{3+} species upon oxidation and incorporated into the Mg(Ni, Fe, Al)O periclase, where the Ni^{2+} and Fe^{3+} species were enriched near the surface. Upon reduction, the surface Ni^{2+} and Fe^{3+} species were reduced from the Mg(Ni, Fe, Al)O periclase to form Ni–Fe alloy nanoparticles again. This structural change was reversible by repeating the oxidation–reduction treatment. This unique property might account for the high sustainability of the Ni–Fe/Mg/Al (Fe/Ni = 0.25) catalyst in the reaction-regeneration cycles.

Similarly, Li et al. prepared a Ni–Cu/Mg/Al bimetallic catalyst by the calcination and reduction of Ni–Cu–Mg–Al HTlcs (Li et al., 2014a). Ni–Cu alloy particles with similar composition and small particle size were formed. The Ni–Cu/Mg/Al catalysts were optimum at the composition of Ni/Cu/Mg/Al = 9.6/2.4/63/25. In addition, the Ni–Cu/Mg/Al catalyst showed better long-term stability than the Ni/Mg/Al catalyst. No obvious aggregation and structural change of the Ni–Cu alloy particles were observed after the reaction. Particularly, the coke deposition on the Ni–Cu/Mg/Al catalyst was approximately ten times smaller than on the Ni/Mg/Al catalyst, demonstrating good coke-resistance of the Ni–Cu alloy particles.

Preparation of Co catalyst from Co–Mg–Al hydrotalcite-like compounds was also attempted (Wang et al., 2014b). It was found that the Co/Mg/Al (10/40/50) catalyst showed much higher activity and resistance to coke deposition than Co/α-Al_2O_3, Co/Al, Co/Mg, and Ni/Mg/Al (9/66/25) catalysts. The high performance of Co/Mg/Al (10/40/50) could be related to the nanocomposite structure consisting of Co metal particles (~14 nm) and oxide particles (~16 nm) of $MgAl_2O_4$-based solid solution. Nevertheless, the Co/Mg/Al catalyst was gradually deactivated by the regeneration treatment due to the structural change of $MgAl_2O_4$-based solid solution to MgO-based solid solution.

Subsequently, Wang et al. reported the preparation of supported Co–Fe alloy particles from Co–Mg–Fe–Al HTlcs (Wang et al., 2014a). Particularly, the Co–Fe alloy nanoparticles have bcc structure at the composition of Co/Fe/Mg/Al = 10/10/40/40, and the composition of each particle was more uniform as compared to that on the Co–Fe/α-Al_2O_3 (Fe/Co = 0.25) catalyst prepared by the impregnation method. It was found that the Co–Fe/Mg/Al (10–10/40/40) catalyst showed higher activity and higher resistance to coke deposition in the SR of tar than the Co–Fe/α-Al_2O_3 (Fe/Co = 0.25), Co/Mg/Al, and Ni–Fe/Mg/Al (Fe/Ni = 0.25) catalysts. In addition, the Co–Fe/Mg/Al (10–10/40/40) catalyst showed higher regenerability than the Co–Fe/α-Al_2O_3 (Fe/Co = 0.25) catalyst in the repeated use. Nevertheless, the decrease in the catalytic performance of Co–Fe/Mg/Al (10–10/40/40) due to the structural change of $MgAl_2O_4$-based solid solution to MgO-based solid solution was also observed. It was thought that the Co–Fe bcc alloy particles on MgO-based solid solution were oxidized more easily than those on $MgAl_2O_4$-based solid solution.

4. Conclusions

Metal catalysts specially Rh, Ni, and Co are promising candidates for steam reforming of tar. Rh is much active and resistant to coke deposition, but its high cost would be the limitation for large-scale application. Ni and Co are cost-effective, but the improvement of catalytic performance including activity, stability, and regenerability is strongly needed. The presence of reducible oxides and addition of second metals are effective to improve the catalytic performances with respect to activity, stability, and resistance to coke deposition and aggregation of metal particles. The metal-oxide and metal–metal interface can play an important role

in determining the catalytic performance by the synergy between the activation of tar on metal and activation of steam on oxide or second metal. The use of hydrotalcite-like precursors is promising to prepare high-performance alloy catalyst with controlled structure, composition, and particle size.

References

Abu El-Rub, Z., Bramer, E.A., Brem, G., 2004. Review of catalysts for tar elimination in biomass gasification processes. Ind. Eng. Chem. Res. 43, 6911–6919.

Asadullah, M., Ito, S., Kunimori, K., Yamada, M., Tomishige, K., 2002. Energy efficient production of hydrogen and syngas from biomass: development of low-temperature catalytic process for cellulose gasification. Environ. Sci. Technol. 36, 4476–4481.

Ashok, J., Kawi, S., 2013. Nickel–iron alloy supported over iron–alumina catalysts for steam reforming of biomass tar model compound. ACS Catal. 4, 289–301.

Bampenrat, A., Meeyoo, V., Kitiyanan, B., Rangsunvigit, P., Rirksomboon, T., 2010. Naphthalene steam reforming over Mn-doped CeO_2–ZrO_2 supported nickel catalysts. Appl. Catal. A: Gen. 373, 154–159.

Basile, F., Albertazzi, S., Barbera, D., Benito, P., Einvall, J., Brandin, J., Fornasari, G., Trifirò, F., Vaccari, A., 2011. Steam reforming of hot gas from gasified wood types and miscanthus biomass. Biomass Bioenergy 1 (Suppl. 35), S116–S122.

Cavani, F., Trifirò, F., Vaccari, A., 1991. Hydrotalcite-type anionic clays: preparation, properties and applications. Catal. Today 11, 173–301.

Colby, J.L., Wang, T., Schmidt, L.D., 2009. Steam reforming of benzene as a model for biomass-derived syngas tars over Rh-based catalysts. Energy Fuels 24, 1341–1346.

Coll, R., Salvadó, J., Farriol, X., Montané, D., 2001. Steam reforming model compounds of biomass gasification tars: conversion at different operating conditions and tendency towards coke formation. Fuel Process. Technol. 74, 19–31.

Constantinou, D.A., Efstathiou, A.M., 2010. Low-temperature purification of gas streams from phenol by steam reforming over novel supported-Rh catalysts. Appl. Catal. B: Environ. 96, 276–289.

Constantinou, D.A., Álvarez-Galván, M.C., Fierro, J.L.G., Efstathiou, A.M., 2012. Low-temperature conversion of phenol into CO, CO_2 and H_2 by steam reforming over La-containing supported Rh catalysts. Appl. Catal. B: Environ. 117–118, 81–95.

Corujo, A., Yermán, L., Arizaga, B., Brusoni, M., Castiglioni, J., 2010. Improved yield parameters in catalytic steam gasification of forestry residue; optimizing biomass feed rate and catalyst type. Biomass Bioenergy 34, 1695–1702.

Draelants, D.J., Zhao, H., Baron, G.V., 2001. Preparation of catalytic filters by the urea method and its application for benzene cracking in H_2S-containing biomass gasification gas. Ind. Eng. Chem. Res. 40, 3309–3316.

Engelen, K., Zhang, Y., Draelants, D.J., Baron, G.V., 2003. A novel catalytic filter for tar removal from biomass gasification gas: improvement of the catalytic activity in presence of H_2S. Chem. Eng. Sci. 58, 665–670.

Furusawa, T., Tsutsumi, A., 2005a. Comparison of Co/MgO and Ni/MgO catalysts for the steam reforming of naphthalene as a model compound of tar derived from biomass gasification. Appl. Catal. A: Gen. 278, 207–212.

Furusawa, T., Tsutsumi, A., 2005b. Development of cobalt catalysts for the steam reforming of naphthalene as a model compound of tar derived from biomass gasification. Appl. Catal. A: Gen. 278, 195–205.

Furusawa, T., Saito, K., Kori, Y., Miura, Y., Sato, M., Suzuki, N., 2013. Steam reforming of naphthalene/benzene with various types of Pt- and Ni-based catalysts for hydrogen production. Fuel 103, 111–121.

Hofbauer, H., Rauch, R., Loeffler, G., Kaiser, S., Fercher, E., Tremmel, H., 2002. Six Years Experience with the FICFB-Gasification Process. 12th Europen Conference and Technology Exhibition on Biomass for Energy, Industry and Climate Protection, Amsterdam, June 2002.

Huber, G.W., Iborra, S., Corma, A., 2006. Synthesis of transportation fuels from biomass: chemistry, catalysts, and engineering. Chem. Rev. 106, 4044–4098.

Kimura, T., Miyazawa, T., Nishikawa, J., Kado, S., Okumura, K., Miyao, T., Naito, S., Kunimori, K., Tomishige, K., 2006. Development of Ni catalysts for tar removal by steam gasification of biomass. Appl. Catal. B: Environ. 68, 160–170.

Koike, M., Li, D., Nakagawa, Y., Tomishige, K., 2012. A highly active and coke-resistant steam reforming catalyst comprising uniform nickel–iron alloy nanoparticles. ChemSusChem 5, 2312–2314.

Koike, M., Hisada, Y., Wang, L., Li, D., Watanabe, H., Nakagawa, Y., Tomishige, K., 2013a. High catalytic activity of Co–Fe/α-Al_2O_3 in the steam reforming of toluene in the presence of hydrogen. Appl. Catal. B: Environ. 140–141, 652–662.

Koike, M., Ishikawa, C., Li, D., Wang, L., Nakagawa, Y., Tomishige, K., 2013b. Catalytic performance of manganese-promoted nickel catalysts for the steam reforming of tar from biomass pyrolysis to synthesis gas. Fuel 103, 122–129.

Kuhn, J.N., Zhao, Z., Senefeld-Naber, A., Felix, L.G., Slimane, R.B., Choi, C.W., Ozkan, U.S., 2008. Ni-olivine catalysts prepared by thermal impregnation: structure, steam reforming activity, and stability. Appl. Catal. A: Gen. 341, 43–49.

Lasa, H., Salaices, E., Mazumder, J., Lucky, R., 2011. Catalytic steam gasification of biomass: catalysts, thermodynamics and kinetics. Chem. Rev. 111, 5404–5433.

Li, B., Watanabe, R., Maruyama, K., Kunimori, K., Tomishige, K., 2005. Thermographical observation of catalyst bed temperature in oxidative steam reforming of methane over Ni supported on α-alumina granules: effect of Ni precursors. Catal. Today 104, 7–17.

Li, C., Hirabayashi, D., Suzuki, K., 2009. A crucial role of O_2^- and O_2^{2-} on mayenite structure for biomass tar steam reforming over Ni/$Ca_{12}Al_{14}O_{33}$. Appl. Catal. B: Environ. 88, 351–360.

Li, D., Nakagawa, Y., Tomishige, K., 2011a. Methane reforming to synthesis gas over Ni catalysts modified with noble metals. Appl. Catal. A: Gen. 408, 1–24.

Li, D., Wang, L., Koike, M., Nakagawa, Y., Tomishige, K., 2011b. Steam reforming of tar from pyrolysis of biomass over Ni/Mg/Al catalysts prepared from hydrotalcite-like precursors. Appl. Catal. B: Environ. 102, 528–538.

Li, D., Ishikawa, C., Koike, M., Wang, L., Nakagawa, Y., Tomishige, K., 2013. Production of renewable hydrogen by steam reforming of tar from biomass pyrolysis over supported Co catalysts. Int. J. Hydrogen Energy 38, 3572–3581.

Li, D., Koike, M., Chen, J., Nakagawa, Y., Tomishige, K., 2014a. Preparation of Ni–Cu/Mg/Al catalysts from hydrotalcite-like compounds for hydrogen production by steam reforming of biomass tar. Int. J. Hydrogen Energy 39, 10959–10970.

Li, D., Koike, M., Wang, L., Nakagawa, Y., Xu, Y., Tomishige, K., 2014b. Regenerability of hydrotalcite-derived nickel–iron alloy nanoparticles for syngas production from biomass tar. ChemSusChem 7, 510–522.

Li, J., Yan, R., Xiao, B., Liang, D.T., Du, L., 2008. Development of nano-NiO/Al_2O_3 catalyst to be used for tar removal in biomass gasification. Environ. Sci. Technol. 42, 6224–6229.

Ma, L., Verelst, H., Baron, G.V., 2005. Integrated high temperature gas cleaning: tar removal in biomass gasification with a catalytic filter. Catal. Today 105, 729–734.

Ma, L., Baron, G.V., 2008. Mixed zirconia-alumina supports for Ni/MgO based catalytic filters for biomass fuel gas cleaning. Powder Technol. 180, 21–29.

Matas Güell, B., Babich, I.V., Lefferts, L., Seshan, K., 2011. Steam reforming of phenol over Ni-based catalysts – a comparative study. Appl. Catal. B: Environ. 106, 280–286.

Mei, D., Lebarbier, V.M., Rousseau, R., Glezakou, V.-A., Albrecht, K.O., Kovarik, L., Flake, M., Dagle, R.A., 2013. Comparative investigation of benzene steam reforming over spinel supported Rh and Ir catalysts. ACS Catal. 3, 1133–1143.

Miyazawa, T., Kimura, T., Nishikawa, J., Kado, S., Kunimori, K., Tomishige, K., 2006. Catalytic performance of supported Ni catalysts in partial oxidation and steam reforming of tar derived from the pyrolysis of wood biomass. Catal. Today 115, 254–262.

Mukai, D., Tochiya, S., Murai, Y., Imori, M., Hashimoto, T., Sugiura, Y., Sekine, Y., 2013. Role of support lattice oxygen on steam reforming of toluene for hydrogen production over Ni/$La_{0.7}Sr_{0.3}AlO_{3-\delta}$ catalyst. Appl. Catal. A: Gen. 453, 60–70.

Mukai, D., Murai, Y., Higo, T., Ogo, S., Sugiura, Y., Sekine, Y., 2014. Effect of Pt addition to Ni/$La_{0.7}Sr_{0.3}AlO_{3-\delta}$ catalyst on steam reforming of toluene for hydrogen production. Appl. Catal. A: Gen. 471, 157–164.

Nacken, M., Ma, L., Engelen, K., Heidenreich, S., Baron, G.V., 2007. Development of a tar reforming catalyst for integration in a ceramic filter element and use in hot gas cleaning. Ind. Eng. Chem. Res. 46, 1945–1951.

Nacken, M., Ma, L., Heidenreich, S., Verpoort, F., Baron, G.V., 2012. Development of a catalytic ceramic foam for efficient tar reforming of a catalytic filter for hot gas cleaning of biomass-derived syngas. Appl. Catal. B: Environ. 125, 111–119.

Nakamura, K., Miyazawa, T., Sakurai, T., Miyao, T., Naito, S., Begum, N., Kunimori, K., Tomishige, K., 2009. Promoting effect of MgO addition to Pt/Ni/CeO_2/Al_2O_3 in the steam gasification of biomass. Appl. Catal. B: Environ. 86, 36–44.

Nishikawa, J., Miyazawa, T., Nakamura, K., Asadullah, M., Kunimori, K., Tomishige, K., 2008a. Promoting effect of Pt addition to Ni/CeO_2/Al_2O_3 catalyst for steam gasification of biomass. Catal. Commun. 9, 195–201.

Nishikawa, J., Nakamura, K., Asadullah, M., Miyazawa, T., Kunimori, K., Tomishige, K., 2008b. Catalytic performance of Ni/CeO_2/Al_2O_3 modified with noble metals in steam gasification of biomass. Catal. Today 131, 146–155.

Oemar, U., Ang, P.S., Hidajat, K., Kawi, S., 2013. Promotional effect of Fe on perovskite $LaNi_xFe_{1-x}O_3$ catalyst for hydrogen production via steam reforming of toluene. Int. J. Hydrogen Energy 38, 5525–5534.

Oemar, U., Ang, M.L., Hee, W.F., Hidajat, K., Kawi, S., 2014. Perovskite $La_xM_{1-x}Ni_{0.8}Fe_{0.2}O_3$ catalyst for steam reforming of toluene: crucial role of alkaline earth metal at low steam condition. Appl. Catal. B: Environ. 148–149, 231–242.

Park, H.J., Park, S.H., Sohn, J.M., Park, J., Jeon, J.K., Kim, S.S., Park, Y.K., 2010. Steam reforming of biomass gasification tar using benzene as a model compound over various Ni supported metal oxide catalysts. Bioresour. Technol. 101, S101–S103.

Peter, M., 2002. Energy production from biomass (part 3): gasification technologies. Bioresour. Technol. 83, 55–63.

Pfeifer, C., Rauch, R., Hofbauer, H., 2004. In-bed catalytic tar reduction in a dual fluidized bed biomass steam gasifier. Ind. Eng. Chem. Res. 43, 1634–1640.

Polychronopoulou, K., Costa, C.N., Efstathiou, A.M., 2004a. The steam reforming of phenol reaction over supported-Rh catalysts. Appl. Catal. A: Gen. 272, 37–52.

Polychronopoulou, K., Fierro, J.L.G., Efstathiou, A.M., 2004b. The phenol steam reforming reaction over MgO-based supported Rh catalysts. J. Catal. 228, 417–432.

Polychronopoulou, K., Bakandritsos, A., Tzitzios, V., Fierro, J.L.G., Efstathiou, A.M., 2006. Absorption-enhanced reforming of phenol by steam over supported Fe catalysts. J. Catal. 241, 132–148.

Polychronopoulou, K., Giannakopoulos, K., Efstathiou, A.M., 2012. Tailoring MgO-based supported Rh catalysts for purification of gas streams from phenol. Appl. Catal. B: Environ. 111–112, 360–375.

Quitete, C.P.B., Bittencourt, R.C.P., Souza, M.M.V.M., 2014. Steam reforming of tar using toluene as a model compound with nickel catalysts supported on hexaaluminates. Appl. Catal. A: Gen. 478, 234–240.

Reed, T.B., 1971. Free energy formation of binary compounds. In: Free Energy Formation of Binary Compounds. MIT Press, Cambridge, MA, pp. 66–67.
Sekine, Y., Mukai, D., Murai, Y., Tochiya, S., Izutsu, Y., Sekiguchi, K., Hosomura, N., Arai, H., Kikuchi, E., Sugiura, Y., 2013. Steam reforming of toluene over perovskite-supported Ni catalysts. Appl. Catal. A: Gen. 451, 160–167.
Swierczynski, D., Courson, C., Bedel, L., Kiennemann, A., Guille, J., 2006. Characterization of Ni–Fe/MgO/olivine catalyst for fluidized bed steam gasification of biomass. Chem. Mater. 18, 4025–4032.
Swierczynski, D., Libs, S., Courson, C., Kiennemann, A., 2007. Steam reforming of tar from a biomass gasification process over Ni/olivine catalyst using toluene as a model compound. Appl. Catal. B: Environ. 74, 211–222.
Tomishige, K., Chen, Y., Fujimoto, K., 1999. Studies on carbon deposition in CO_2 reforming of CH_4 over nickel–magnesia solid solution catalysts. J. Catal. 181, 91–103.
Tomishige, K., Kimura, T., Nishikawa, J., Miyazawa, T., Kunimori, K., 2007. Promoting effect of the interaction between Ni and CeO_2 on steam gasification of biomass. Catal. Commun. 8, 1074–1079.
Wang, D., Yuan, W., Ji, W., 2011a. Char and char-supported nickel catalysts for secondary syngas cleanup and conditioning. Appl. Energy 88, 1656–1663.
Wang, L., Li, D., Koike, M., Koso, S., Nakagawa, Y., Xu, Y., Tomishige, K., 2011b. Catalytic performance and characterization of Ni–Fe catalysts for the steam reforming of tar from biomass pyrolysis to synthesis gas. Appl. Catal. A: Gen. 392, 248–255.
Wang, L., Hisada, Y., Koike, M., Li, D., Watanabe, H., Nakagawa, Y., Tomishige, K., 2012. Catalyst property of Co–Fe alloy particles in the steam reforming of biomass tar and toluene. Appl. Catal. B: Environ. 121–122, 95–104.
Wang, L., Li, D., Koike, M., Watanabe, H., Xu, Y., Nakagawa, Y., Tomishige, K., 2013. Catalytic performance and characterization of Ni–Co catalysts for the steam reforming of biomass tar to synthesis gas. Fuel 112, 654–661.
Wang, L., Chen, J., Watanabe, H., Xu, Y., Tamura, M., Nakagawa, Y., Tomishige, K., 2014a. Catalytic performance and characterization of Co–Fe bcc alloy nanoparticles prepared from hydrotalcite-like precursors in the steam gasification of biomass-derived tar. Appl. Catal. B: Environ. 160–161, 701–715.
Wang, L., Li, D., Watanabe, H., Tamura, M., Nakagawa, Y., Tomishige, K., 2014b. Catalytic performance and characterization of Co/Mg/Al catalysts prepared from hydrotalcite-like precursors for the steam gasification of biomass. Appl. Catal. B: Environ. 150–151, 82–92.
Wang, T., Chang, J., Cui, X., Zhang, Q., Fu, Y., 2006. Reforming of raw fuel gas from biomass gasification to syngas over highly stable nickel–magnesium solid solution catalysts. Fuel Process. Technol. 87, 421–428.
Xiao, X., Meng, X., Le, D.D., Takarada, T., 2011. Two-stage steam gasification of waste biomass in fluidized bed at low temperature: parametric investigations and performance optimization. Bioresour. Technol. 102, 1975–1981.
Xu, C., Donald, J., Byambajav, E., Ohtsuka, Y., 2010. Recent advances in catalysts for hot-gas removal of tar and NH_3 from biomass gasification. Fuel 89, 1784–1795.
Yamazaki, O., Tomishige, K., Fujimoto, K., 1996. Development of highly stable nickel catalyst for methane-steam reaction under low steam to carbon ratio. Appl. Catal. A: Gen. 136, 49–56.
Yung, M.M., Jablonski, W.S., Magrini-Bair, K.A., 2009. Review of catalytic conditioning of biomass-derived syngas. Energy Fuels 23, 1874–1887.
Zhao, H., Draelants, D.J., Baron, G.V., 2000a. Performance of a nickel-activated candle filter for naphthalene cracking in synthetic biomass gasification gas. Ind. Eng. Chem. Res. 39, 3195–3201.
Zhao, H., Draelants, D.J., Baron, G.V., 2000b. Preparation and characterisation of nickel-modified ceramic filters. Catal. Today 56, 229–237.
Zhao, Z., Kuhn, J.N., Felix, L.G., Slimane, R.B., Choi, C.W., Ozkan, U.S., 2008. Thermally impregnated Ni–olivine catalysts for tar removal by steam reforming in biomass gasifiers. Ind. Eng. Chem. Res. 47, 717–723.
Zhao, Z., Lakshminarayanan, N., Kuhn, J.N., Senefeld-Naber, A., Felix, L.G., Slimane, R.B., Choi, C.W., Ozkan, U.S., 2009. Optimization of thermally impregnated Ni–olivine catalysts for tar removal. Appl. Catal. A: Gen. 363, 64–72.